GPR and Geoelectrical Surveys at a Patagonian Archaeological Site. Part II: Numerical Simulations

M. de la Vega, Osella A., Lascano E. – Buenos Aires University, Argentina
J. M Carcione – Istituto Nazionale di Oceanografia e di Geofisica Sperimentale (OGS), Italy

Abstract

Part I of this work deals with the acquisition, processing and interpretation of geophysical data acquired at the Floridablanca archaeological site, where remains of ancient Spanish buildings are buried. The techniques used in the survey are the geo-electric and ground-penetrating-radar methods. Use of inversion algorithms alone to interpret the data has not been conclusive to obtain a reliable model, since many uncertainties remained in the interpretation. Hence, in Part II we make use of forward-modeling methods to simulate the low- and high frequency electromagnetic responses of the structures to aid the interpretation. The simulations allow us to improve the model, regarding the location and size of the adobe walls making the buildings.

Introduction

Lascano et al. (2003) (Part I) present a preliminary interpretation of the data obtained at the Floridabanca archaeological site using geophysical techniques. The study focus on one sector of the site called North Wing I (NWI). The objective of the prospection is to determine the internal structure of the settler's houses. In order to do this, three different geophysical methods were applied: Ground Penetrating Radar (GPR), Resistivity Method and Electromagnetic Induction Method (EMI). The analysis reveals a number of anomalies, which after correlation with the archaeological and historical information available, can be associated to adobe or similar raw-material walls. These anomalies present a periodic distribution which indicate that the NWI sector corresponds to a main structure composed by substructures, each one divided by an inner and narrower wall.

We use geophysical data as well as information from excavations as a starting point for modeling the response of the different structural features. Resistivity and GPR forward modeling is performed. Moreover, we determine the resolution of both methods to detect different combinations of buried walls. Finally, we correlate the simulations to the data in order to obtain a better interpretation of the anomalies and improve the resolution of future geophysical surveys.

Data

In Fig. 1 a) and b) an inner or internal wall and a wider or separation wall (marked with a dashed line) of one house excavated in another sector of the site are shown respectively.

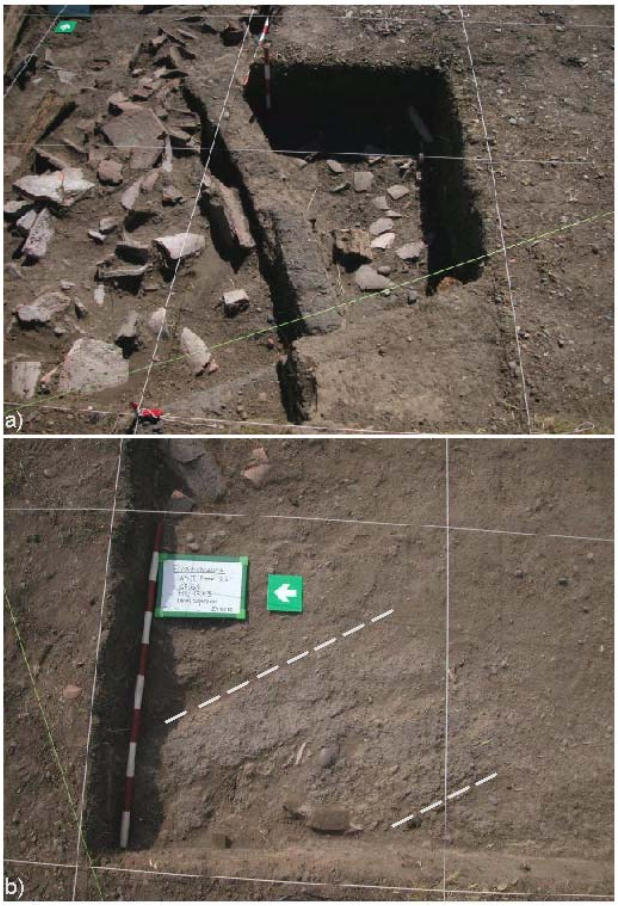

Figure. 1: a) an internal or inner wall and b) a wider separation wall excavated in another sector of the site. The excavated separation wall is marked with a dashed line.

Part of the geophysical data of the NWI sector are shown in Fig. 2. These data correspond to Fig. 2 of Part I of this work. The separation between the strong anomalies can be estimated in 7 m approximately. The difference in the strength of the anomalies could be an indicator of the presence of different types of walls along the profile. The stronger anomalies would correspond to the walls separating consecutive houses (separation walls) and the weaker ones to the inner walls.

The geo-electrical profiles present interesting results. A resistive structure up to a depth of 1.5 m is clearly detected, and a periodic pattern is observed (see Fig. 2a). As can be appreciated, the location of these anomalies coincides with those observed in the corresponding radargram (Fig. 2b).

Summarizing, we may conclude that the anomalies found with both methods can be due to different kind of buried structures. Nevertheless, many questions remain unsolved. For example, it is not clear if the differences in the strength between the anomalies correspond to different kind of walls (thinner or thicker walls) or to the presence of collapsed walls. In order to reduce these uncertainties, we simulate the GPR and geo-electric responses for different cases.

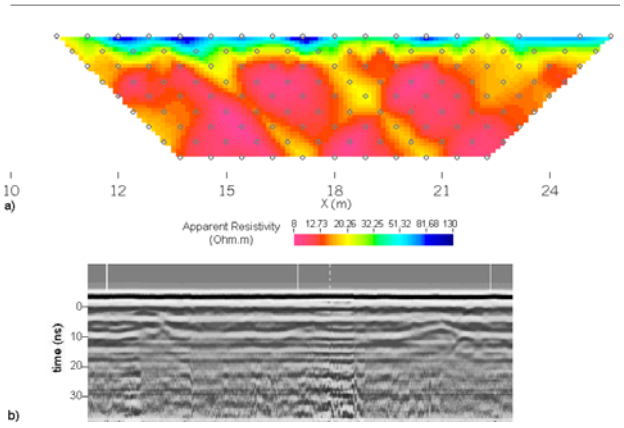

Figure 2: Experimental data. a) Resistivity pseudosection, b) Radargram

Modeling

The geo-electrical data inversion of the selected data studied here (see Fig. 6 in Part I) show that the subsurface structure proposed to be the cause of the detected anomalies consists of a sedimentary layer of nearly 85 cm thick, formed by clayey sand with relative permittivity equal to 4 and conductivity equal to 0.02 S/m. Below this layer, there is layer of wet clay with relative permittivity equal to 10 and conductivity equal to 0.1 S/m. The top of the adobe walls are situated in the sedimentary layer at a depth of 12 cm and the height of these walls is 60 cm. Two major walls, constituting the house boundaries (separation walls), are 7 m apart and have a width of 40 cm, and a minor block of 20 cm width represents an inner wall located at 4 m from the leftward wider wall. The adobe walls have a relative permittivity equal to 2 and conductivity equal to 0.003 S/m. This subsurface structure is named case A. Another three cases are variations of this model: case B, the middle wall is absent; case C, the middle wall has collapsed to the left side; and case D, the height of the middle wall has been halved.

GPR radiation patterns (corresponding to a 500 MHz antenna) and resistivity electrode deployments (with electrode apertures of 0.8 m) are simulated according to the field-work experimental characteristics (see Part I).

Radargrams

The radar simulations are based on the forward modeling code developed by Carcione (1996a,b,c) using the Fourier pseudospectral method. The simulation uses a numerical mesh of 1080 x 160 grid points, with a grid spacing of 1 cm. (20 grid points at the sides and bottom of the mesh are used to absorb the wave field exiting the model). The source is a Ricker-type wavelet with a dominant frequency of 500 MHz, applied as a vertically propagating plane wave to approximate a mono-static survey. The source is located at the air/sand interface, and has horizontal polarization. The 2-D numerical modeling algorithm uses a time step of 0.01 ns.

Resistivity Pseudosections

The geoelectrical simulation is performed with the DCIPF2D program developed by the University of British Columbia and based on the work of Oldenburg et al. (1193) and Oldenburg and Li (1994). This program computes DC potentials be means of a finite difference technique, and we use a numerical mesh of 106 x 34 grid points, with a grid spacing of 20 cm.

Geoelectrical and GPR Results

Case A: two separation walls 7 m apart and an inner wall 3 m to the left of the last wall. The separation walls are centered at x = 3.2 m and x = 10.2 m, and the inner wall at x = 7.1 m, respectively.

In Fig. 3a) the anomalies generated by each buried wall can clearly be seen as higher apparent resistivity values. The shape of the anomalies is not the same for identical walls, because it depends on the relative position of the electrodes and the wall. The wider walls (separation walls) present a stronger anomaly than the thinner wall (inner wall) as it is expected. For both the inner and the right external wall, the anomaly is shifted between 0.8 and 1.6 m from the actual position of the wall.

The presence of the buried walls can also be detected from the deeper points of the profile. The uniform conductive layer (apparent resistivity of approximately 10 Ω.m) is interrupted by more resistive points aligned along inclined lines (apparent resistivity of approximately 15 Ω.m) that form an inverted V underneath each wall.

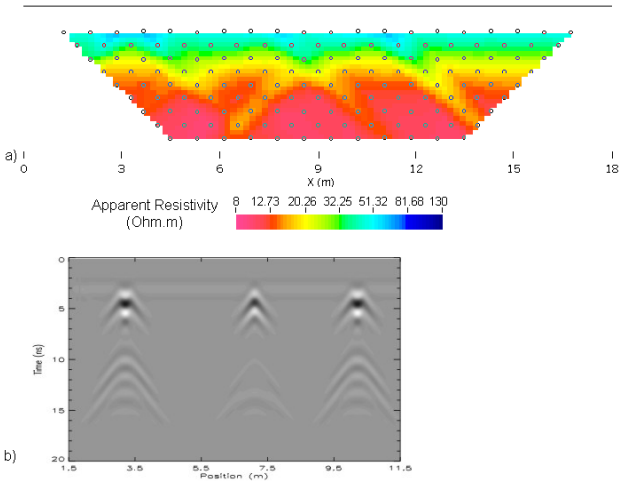

Figure 3: Case A simulation. a) Modeled resistivity pseudosection, b) Synthetic radargram

The synthetic radargram is shown in Fig. 3b. We observe the direct wave till approximately 2 ns, the reflected wave from the sand/clay interface at approximately 14 ns, and the responses of the walls at the expected horizontal locations. The diffraction-reflection hyperbolae generated by the walls are clear at 4 ns and between 8 and 13 ns. At the location of the walls, the reflection from the sand/clay interface arrives in advance, due to the higher electromagnetic velocity of the walls compared to that of the sand.

Case B: two separation walls 7 m apart from each other and no inner wall.

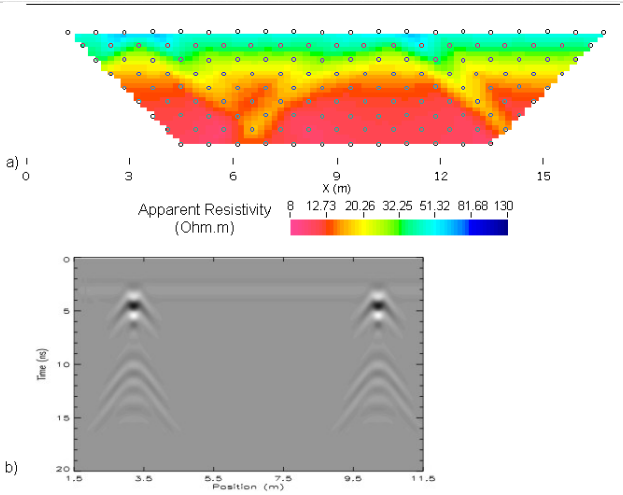

Figure 4: Case B simulation. a) Modeled resistivity pseudosection, b) Synthetic radargram

Fig 4a shows the apparent resistivity profile corresponding to case B. The two buried walls can be distinguished. This case shows a different behavior compared to the first resistive profile. So, the presence or absence of an inner wall can clearly be determined.

As in the previous case, the presence of the walls can be detected because of the inverted V feature mentioned above. In this case, it is clear below the external wall located at X = 10 m.

The synthetic radargram is shown in Fig. 4b. We observe a similar response, regarding external walls, to that of Fig. 3b. The walls are very well resolved, with no appreciable interference in the region between them..

Case C: two separation walls 7 m apart, and the inner wall collapsed to the left side.

Fig. 5a shows the aparent-resistivity simulation corresponding to case C. The response of the collapsed inner wall is clear, but the anomaly and contrast with the surrounding medium are much weaker than in Case A.

The synthetic radargram shown in Fig. 5b has a similar behavior of that of case B, but after 9 ns the response of the collapsed wall can be seen. This wall has been modeled as a block of 20 cm height and 60 cm width. Then, the response is wider than in the other cases.

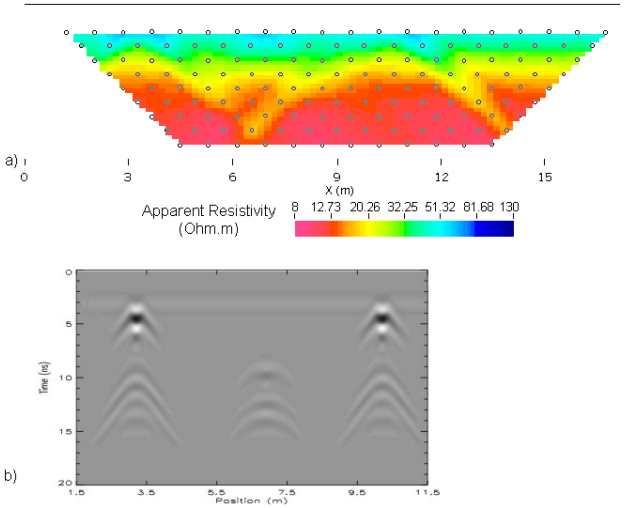

Figure 5: Case C simulation. a) Modeled resistivity pseudosection, b) Synthetic radargram

Case D: two separation walls 7 m apart, and the height of the middle wall has been halved.

In this case, the height of the inner wall is 30 cm, instead of 60 cm. The geo-electric simulation shows that in this case the wall cannot be resolved, so a shorter wall cannot be detected, at least for the electrode aperture used in this simulation.

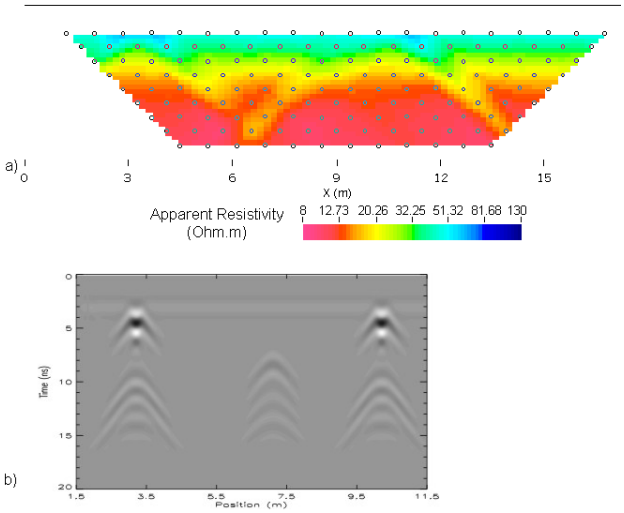

Figure 6: Case D simulation. a) Modeled resistivity pseudosection, b) Synthetic radargram

The synthetic radargram is shown in Fig. 6b. The difference with the radargram obtained for the collapsed wall is clear, both in the location of the top of the reflection hyperbola (approximately 7 ns) and in its width.

Though there is only a difference of 10 cm between the height of the collapsed wall (20 cm) and this case (half height wall of 30 cm), the shift in time of the anomaly can clearly be appreciated.

Two more simulations (cases E and F) are performed to analyze the apparent resistivity and radargram corresponding to the last two cases, when more resolution is used. These simulations are similar to the two previous ones but with an electrode separation of 0.5 m for resistivity simulations and a dominant frequency of 1 GHz for the GPR simulations.

Case E: two separation walls 7 m apart, and the inner wall collapsed to the left side.

Case F: two separation walls 7 m apart, and the height of the middle wall has been halved.

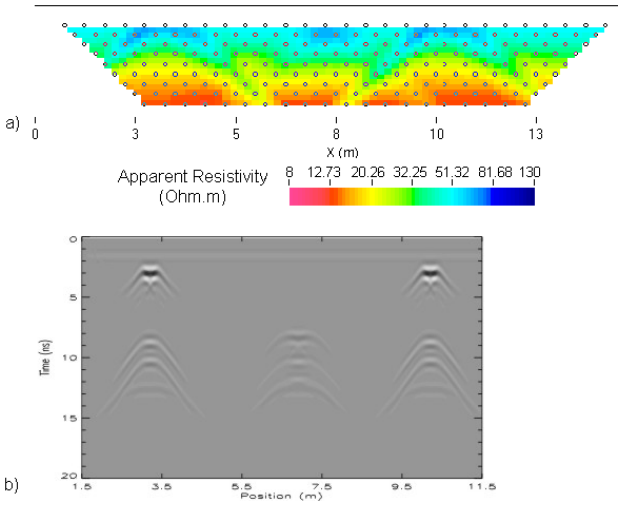

Figure 7: Similar to Case C but with higher resolution. a) electrode separation = 0.5 m, b) frequency = 1 GHz

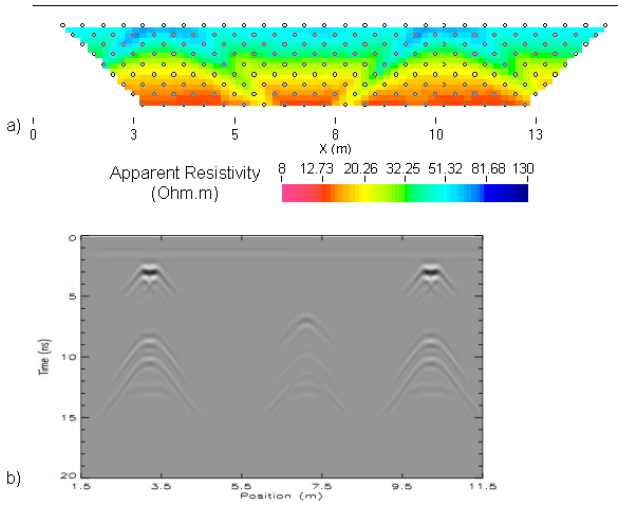

Figure 8: Similar to Case D but with higher resolution. a) electrode separation = 0.5 m, b) frequency = 1 GHz

The apparent resistivity profiles for both cases (Figs. 7a and 8a, respectively) are, as expected, clearer than for an electrode aperture of 0.8 m. But despite this fact, this electrode aperture does not improve very much the resolution of the profile. In case E, the inner wall still remains unseen by the configuration. Also, the lower conductive layer is not well defined. So, although this electrode aperture allows us to distinguish the buried walls more clearly, we cannot obtain information about the medium in which the buried structures are embedded.

The corresponding radargrams (Figs. 7b and 8b, respectively) reveal a similar behavior as the previous ones. A better resolution is achieved for the first reflections, especially in the definition of the vertical dimension of the walls.

Discussion and Conclusions

Different structures have been simulated to model the adobe walls buried at the Floridablanca archaeological site. The results obtained from the simulation of GPR and geo-electrical data allow us to conclude that using both methods in a convenient way, the walls can be differentiated in spite of the low resistivity contrast with the surrounding media.

Comparing the geo-electrical simulations with the field data, we can see that the resolutions coincide This result can be achieved with a convenient combination of electrode apertures. On the contrary, if we observe the real and the synthetic radargrams, a clear difference appears. Although the reflections due to the first interface are very similar, the reflection corresponding to the bottom of the walls are weaker in the real data.

The GPR synthetic response is sensitive to the dimensions of the walls; this sensitivity may be improved by using a higher frequency antenna (1 GHz), but nevertheless the resolution of the 500 MHz antenna allows an acceptable detection of the walls.

Similarly, the geo-electrical response also distinguishes the walls and has enough sensitivity to recognize the inner and major walls. Again, the sensitivity may be improved by decreasing the electrode apertures, but in this case, the lower aperture implies lower penetration. Then, a combined geometry should be used in order to have better lateral resolution with deep penetration.

Acknowledgments

This work was partially supported by ANPCyT (Agencia Nacional de Promoción Científica y Tecnológica).

References

Carcione, J. M., 1996a. Ground penetrating radar: wave theory and numerical simulation in lossy anisotropic media. *Geophysics* 61: 1664-1677.

Carcione, J. M., 1996b. Ground radar simulation for archaeological applications, *Geophys. Prosp*. 44: 871-888.

Carcione, J. M., 1996c. Ground-radar numerical modelling applied to engineering problems, European *Journal of Environmental and Engineering Geophysics* 1: 65-81.

DCIP2D V3.2, 2000. Forward Modelling and Inversion of DC Resistivity and Induced Polarization Data over 2D Structures. UBC-Geophysical Inversion Facility.

Lascano E., Osella A., and de la Vega, M., 2003. GPR and Geoelectrical Surveys at a Patagonian Archaeological site. Part I: Data Analysis, 8th Inter. Congress, Braz. Geophys. Soc., submitted.

Oldenburg, D. W., McGillivary, P. R. and Ellis, R. G., 1993. Generalized subspace method for large scale inverse problems. *Geophys. J. Int.*, **114**, 12-20.

Oldenburg, D. W. and Li, Y., 1994. Inversion of induced polarization data. *Geophysics*, **59**, 1327-1341.